International Symposium
On Turbulence and Shear Flow
Phenomena (TSFP-8)
August 28 - 30, 2013 Poitiers, France

DIRECT NUMERICAL SIMULATION OF TURBULENT MIXING LAYERS WITH PERIODIC FORCING INDUCED INFLOW

Yukinori Kametani
Department of Mechanical Engeneering
Keio University
Yokohama 223-8522, Japan
kametani@fukagata.mech.keio.ac.jp

Masayuki Kawagoe
Department of Mechanical Engeneering
Keio University
Yokohama 223-8522, Japan
kawagoe@fukagata.mech.keio.ac.jp

Koji Fukagata
Department of Mechanical Engeneering
Keio University
Yokohama 223-8522, Japan
fukagata@fukagata.mech.keio.ac.jp

ABSTRACT

The direct numerical simulation of the turbulent mixing layer with periodically-forced inflow is performed. The angular frequency Ω_c was set as a control parameter. To compare the experimental study of Naka *et al.* (2010), the angular frequency is set to be $\Omega = 0.83$ (Case A) and 3.85 (Case B). In the present simulation, the momentum thickness shows the Case A achieved the mixing enhancement, while Case B achieves its suppression. Due to the both controls, the Reynolds normal shear stress, especially $\overline{v'v'}$ increases behind the periodic forcing. The Reynolds shear stress $\overline{u'v'}$ is suppressed in the Case B at downstream. This region is agree with that the mixing suppression is found in the momentum thickness. Furthermore, the anisotropic tensor indicates that two dimensional large coherent structure is generated in the Case B in which mixing was suppressed.

Introduction

A mixing layer is one of the fundamental free shear flow generated by the velocity gap (Brown & Roshko (2009)). In order to understand the vortex dynamics in shear flows, mixing layers have extensively been studied since Brown & Roshko (1974) experimentally visualized the coherent structure in turbulent mixing layers. Huang & Ho (1990) experimentally studied an acoustically perturbed laminar mixing layer and observed small-scale turbulence created due to interaction of spanwise and streamwise structures after the merging of spanwise vortices.

Turbulent mixing layers can be found in various practical applications: e.g., inside combustion chambers and around the exhaust of turbo engines. Techniques for mixing enhancement or suppression are sometimes needed for efficient combustion or noise reduction. Ho (1982) attempted to control the mixing layer by perturbing the flow rates of inflows. They show that the spreading rate of a mixing layer can be manipulated at very low forcing level if the mixing layer is perturbed near a subharmonic of the most-amplified frequency. Naka *et al.* (2010) studied a mixing layer periodically forced by using a flap-type actuator made of piezo-plastic (Polyvinylidene fluoride: PVDF) film aiming at both enhancement and suppression of mixing. They conclude that at some parameters of forcing mixing suppression can also be achieved.

In the present study, direct numerical simulation (DNS) of turbulent mixing layers with periodic forcing, which mimics that by the flap-type actuator of Naka *et al.* (2010), is performed. The forcing by the flap-type actuator is modeled by transversely oscillating the inflow turbulent boundary layers.

Direct numerical simulation

The governing equations are the incompressible continuity and Navier-Stokes equations as following,

$$\frac{\partial u_i}{\partial x_i} = 0, \tag{1}$$

$$\frac{\partial u_i}{\partial t} = -\frac{\partial u_i u_j}{\partial x_j} - \frac{\partial p}{\partial x_i} + \frac{1}{Re}\frac{\partial^2 u_i}{\partial x_j \partial x_j}, \tag{2}$$

where x_i $(i = 1, 2, 3)$ are the Cartesian coordinates u_i are the corresponding velocity components. All variables are non-dimensionalized by the free-stream velocity, 99% boundary layer thickness of the induced turbulent boundary layer in the low-speed side, denoted as U_L and δ, respectively. The inlet profiles of velocities are prepared by performing DNS of turbulent boundary layer (Kametani & Fukagata, 2011) in advance, in which the recycle method uses (Lund *et al.*, 1998). The DNS code is based on a channel flow code developed by Fukagata *et al.* (2006). The spatial discretization uses the energy-conservative second-order finite difference scheme (e.g., Ham *et al.* (2002)). The time integration uses the low-storage third-order Runge-Kutta/Crank-Nicolson scheme (e.g., Spalart *et al.* (1991)). The free-steam velocity in high speed-side is twice faster than that in low speed-side. The convective boundary condition is

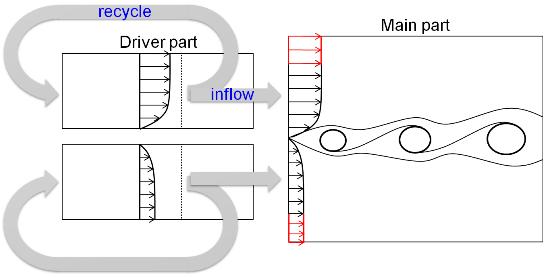

Figure 1. Computational domain

applied at the outlet of the computational domain as

$$\frac{\partial u_i}{\partial t} + U_c \frac{\partial u_i}{\partial x} = 0, \quad (3)$$

where U_c denotes the average of free-stream velocities in the high-speed side and low-speed side, viz., $U_c = 1.5$. The pressures at the inlet and outlet boundaries are given by the Navier-Stokes characteristic boundary condition (NSCBC) of Miyauchi *et al.* (1996),

$$\frac{\partial p}{\partial t} + U_c \frac{\partial p}{\partial x} = \frac{1}{2Re}\omega_z^2, \quad (4)$$

where ω_z denotes the spanwise vorticity. It is known that this boundary condition considerably suppresses the unphysical pressure near the inlet and outlet that appears when an ordinary Neumann condition is used.

The computational domain consists of $0 \le x \le 3\pi$ in the streamwise direction, $-10 \le y \le 10$ in the vertical direction, and $0 \le z \le \pi$ in the spanwise direction, respectively. The correspond grid numbers are $(N_x, N_y, N_z) = (128, 224, 128)$. The grid spacings in the streamwise and spanwise directions are $\Delta x = 7.36 \times 10^{-2}$ and $\Delta z = 2.45 \times 10^{-2}$, respectively. The minimum grid spacing in the transverse direction is $\Delta y = 0.3 \times 10^{-2}$ and the maximum spacing is $\Delta y = 0.41$.

To prepare the inflow velocity profiles, the DNS of turbulent boundary layer is performed with different two Reynolds numbers, corresponding U_L and U_H. The computational domain for turbulent boundary layer consists of $0 \le x^D \le 3\pi$ in the streamwise direction, $0 \le y^D \le 3$ in the vertical direction, and $0 \le z^D \le \pi$ in the spanwise direction, respectively, where superscript D denotes the inflow driving region. The corresponding numbers of grid points are $(N_x^D, N_y^D, N_z^D) = (128, 96, 128)$.

Figure 1 shows the schematic computational domain in the present study. The inlet flows are assumed to be split by the thin plate. The friction Reynolds number of the induced velocity in the low speed side, Re_τ^L, is $Re_\tau^L \approx 160$.

Periodic forcing

As mentioned above, the inlet velocity profile consists of two inlet profiles of turbulent boundary layers. The inlet profile is periodically oscillated by transforming the coordinate as

$$y(t) = y - A\sin(\Omega_c t), \quad (5)$$

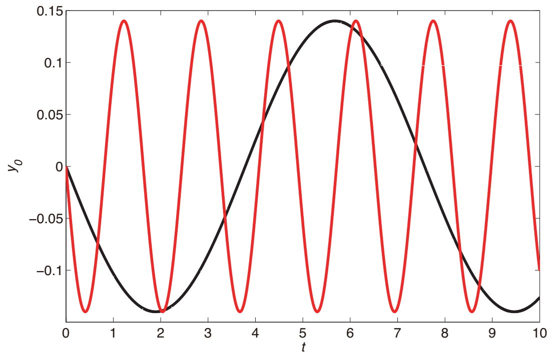

Figure 2. The transition of the boundary of inlet velocity profiles periodically forced.

where A and Ω_c denote the forcing amplitude and the angular frequency as control parameters, respectively. In this study, owing to mimic the forcing by PVDFs in the experiment of Naka *et al.* (2010), the amplitude is fixed to $A = 0.14$ and the angular frequencies are set to be $\Omega_c = 0.83$ and 3.87. The present forcing conditions are listed in Table 1. Figure 2 shows that the time-marching transverse position of the boundary of high speed and low speed velocity profiles. It is confirmed that, the inlet velocity profiles are periodically oscillated.

Result and Discussion

Vortex structures

The instantaneous flow fields of each case are depicted by the pressure (gray iso-surface) and the second invariant of velocity-gradient tensor (red iso-surface) in Fig.3. These iso-surfaces show the vortices and blade region, respectively. In the uncontrolled case, the two-dimensional spanwise vortices are generated at the inlet and it breaks down as it flows downstream. It can be seen the turbulent structures in the blade region where the shear stress is dominant. In the Case A, the spanwise large vortex at the inlet seems to grow in downstream direction due to the periodic forcing. With more higher frequency of forcing in Case B, the spanwise roller structure appears at equal intervals. The blade region is clarified by the forcing compared to the other two cases. Although the roller vortices become smaller as they flow downstream, the roller structure sustains its form.

Statistics

To see the effect of the periodic forcing, the spatial development of the turbulent mixing layer is examined with

Table 1. Forcing conditions

	Forcing		
Case	Uncontrolled	A	B
Angular frequency, Ω_c	0	0.83	3.85
Frequency, f_c	-	0.182	0.615
Wave length, λ	-	11.4	2.44
Period, T	-	7.58	1.63

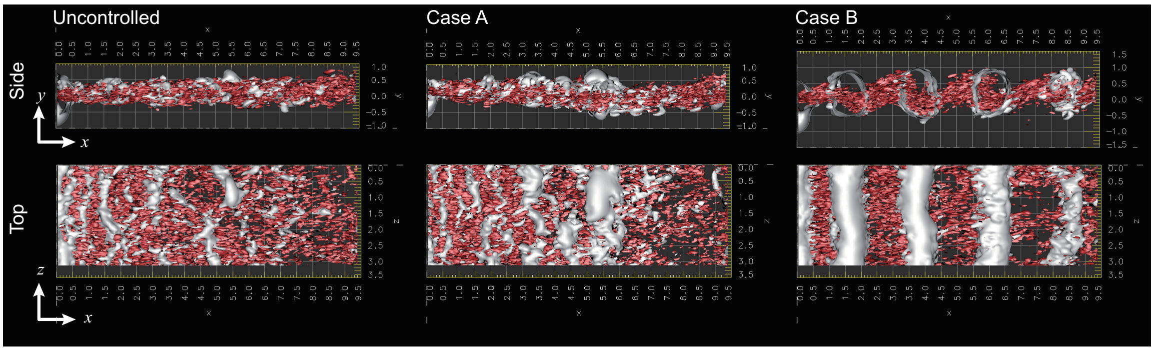

Figure 3. Vortical structures: white, the iso-surface of pressure; red, the iso-surface of second invariant of velocity-gradient tensor.

the momentum thickness θ and vorticity thickness δ_ω calculated as

$$\theta = \frac{1}{\Delta U^2}\int_{-\infty}^{\infty}(U_H - U(y))(U(y)-U_L)\,dy, \quad (6)$$

$$\delta_\omega = \frac{\Delta U}{\partial U/\partial y|_{\max}}, \quad (7)$$

where ΔU denotes the gap between free stream velocities in high-speed side and low-speed side, viz., $\Delta U = U_H - U_L$. Figure 4 and 5 depict the momentum thickness and the vorticity thickness in the present simulation with those from experiment of Naka *et al.* (2010). Here, θ_0 and $\delta_{\omega,0}$ denote the most upstream value of uncontrolled case from the experiment. The momentum thickness develops in downstream direction in all cases. Both of the controlled cases are thicken the momentum thickness compared to the uncontrolled case, although its grow-rate becomes smaller at downstream in Case B. The momentum thickness of uncontrolled case has good agreement with that from the experiment. In the Case A and B, however, there are large differences between the profile from present simulation and that from the experiment. Similarly, the vorticity thickness in the periodically forced cases are not agree with those in the experiment. As for Case B, the thickness becomes thinner than uncontrolled case. Although the forcing condition is exactly equal, the gap is still large in Case A. The difference in the Reynolds number, the inflow condition or the numerical boundary conditions might cause these gap between them. Due to the numerical result, both of momentum and vorticity thickness are increased in the both of Case A and B. Although vorticity thickness is decreased to less than that of uncontrolled case after $x \approx 4$ in Case B, it is still unclear wether mixing is suppressed or not because of the short streamwise computational domain length.

Figure shows the mean streamwise velocity in each case. It is found that, in the present simulation, the mixing layer does not achieve fully developed turbulent condition since the momentum deficit in inlet boundary layer remains at the downstream end of the computational domain. Other remarkable difference appears in the gradient of the velocity near the center which approximately correspond to the vorticity thickness. Compared to that in uncontrolled case and Case A, the velocity-gradient in the Case B shows the slow spatial development, while the momentum deficit decreases faster than the other cases.

Figure and **??** show streamwise and transverse Reynolds normal stresses, $\overline{u'u'}$ and $\overline{v'v'}$. It can be seen that $\overline{u'u'}$ is enhanced by the control. It, however, suppressed as far as $x = 1$. Comparing the Case A with Case B, $\overline{u'u'}$ in the Case B seems to be more diffused than that in the Case A in the range of $1 \le x \le 7$. On the other hand, $\overline{v'v'}$ is suppressed in the Case A, while it increases in Case B. It is also found that $\overline{v'v'}$ is drastically enhanced in the region of $0 \le x \le 6$ and $-0.5 \le y \le 0.5$ in Case B, while it decreases at the more downstream region.

The Reynolds shear stress (RSS), $\overline{u'v'}$, is depicted in Fig.9. Compared to uncontrolled case, $\overline{u'v'}$ is decreased

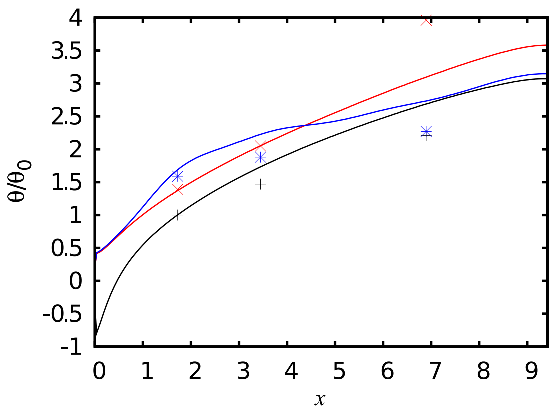

Figure 4. The momentum thickness: solid line, present DNS; markers, experiment of Naka *et al.* (2010): black, uncontrolled; red, Case A; blue, Case B.

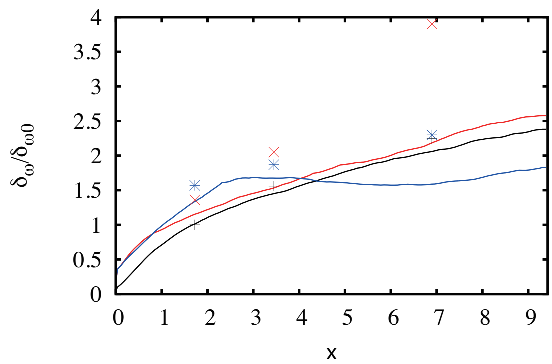

Figure 5. The vorticity thickness: solid line, present DNS; markers, experiment of Naka *et al.* (2010): black, uncontrolled; red, Case A; blue, Case B.

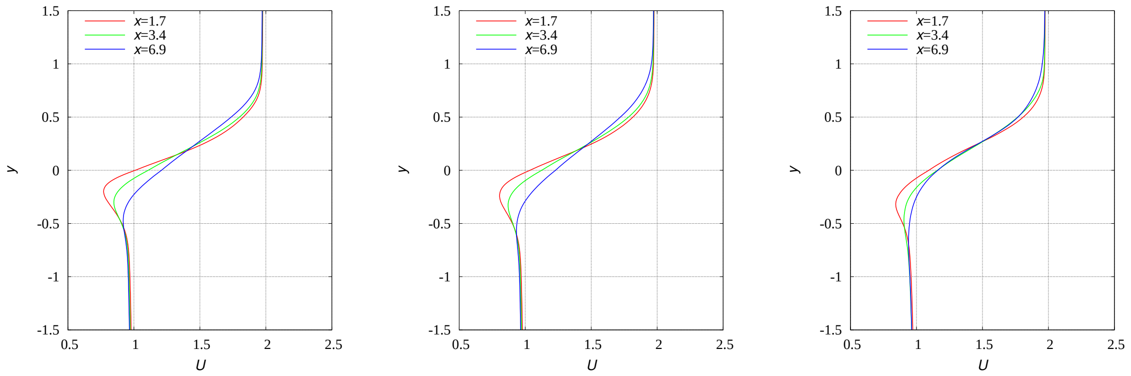

Figure 6. Mean streamwise velocity: left, Uncontrolled; center, Case A; right, Case B.

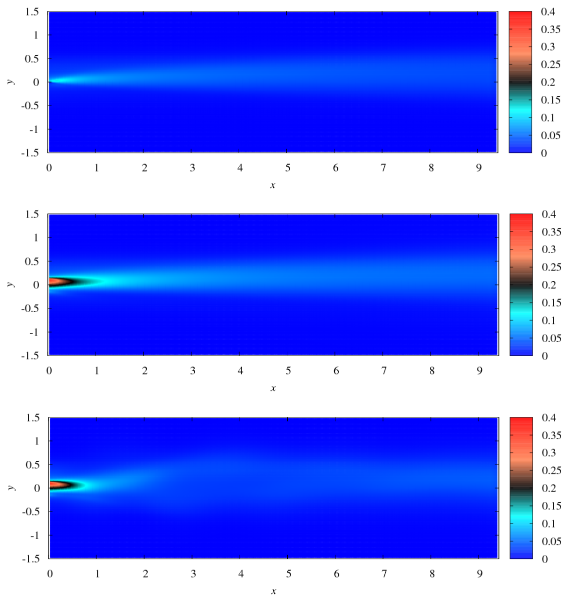

Figure 7. Streamwise Reynolds normal stress, $\overline{u'u'}$: top, uncontrolled; middle, Case A; bottom, Case B.

from upstream of the computational domain. The interesting effect of the control appears in the Case B. In the Case B, it is found that, after $\overline{u'v'}$ is enhanced in the range of $0 \leq x \leq 3$, it is drastically suppressed and diffused in the range of $3 \leq x \leq 7$. At more downstream, the RSS seems to recover again. The reduction of $\overline{u'v'}$ means that the correlation between streamwise and transverse turbulence is decreased. The region in which the RSS is enhanced agrees with that in which the development of momentum thickness is delayed.

To know the figure of the turbulence in the turbulent mixing layer, the second and third invariant of anisotropy tensor at downstream of the low speed-side $(-10 \leq y \leq 0)$ are plotted in Fig.10. From the result, the profile of Case A approaches that of the uncontrolled case. On the other hand, wider two dimensional region appears in Case B compared with other cases since the large coherent structure, shown in Fig. 3, is produced by the control.

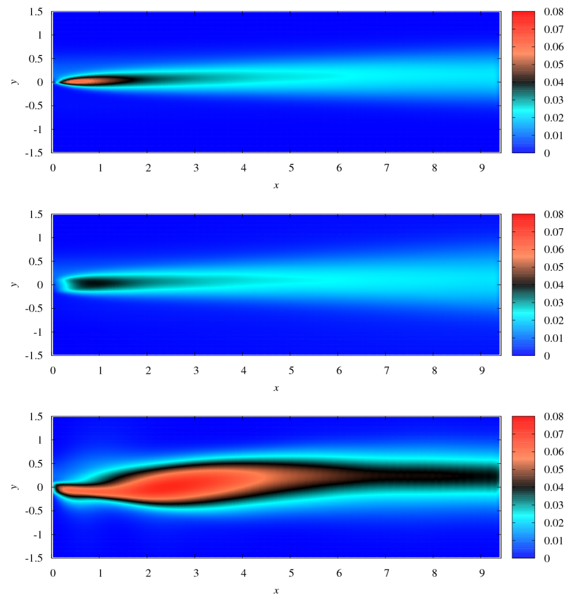

vv)

Figure 8. Transverse Reynolds normal stress, $\overline{v'v'}$: top, uncontrolled; middle, Case A; bottom, Case B.

Conclusion

The direct numerical simulation of the turbulent mixing layer with periodically-forced inflow was performed. The control parameter, nondimensional forcing frequency Ω_c, was set to be 0 (Uncontrolled), 0.83 (Case A) and 3.85 (Case B). From the momentum thickness, the periodic forcing at the inlet enhanced mixing. In the Case B, however, mixing is suppressed by the control downstream, while mixing is enhanced upstream. The Reynolds shear stress is suppressed in the same region where the development of the momentum thickness was suppressed, while the streamwise and transverse Reynolds normal stresses are enhanced. In the present study, the Case A and the Case B achieved the mixing enhancement and suppression, respectively. But the agreement between the present simulation and experiment (Naka *et al.*, 2010) was not found due to the deference in inlet velocity profiles or the short length of computational domain, especially in streamwise direction. In addition, for more deep analysis of the mechanism of the mixing enhancement or suppression, the budget of the turbulent kinetic energy should be considered.

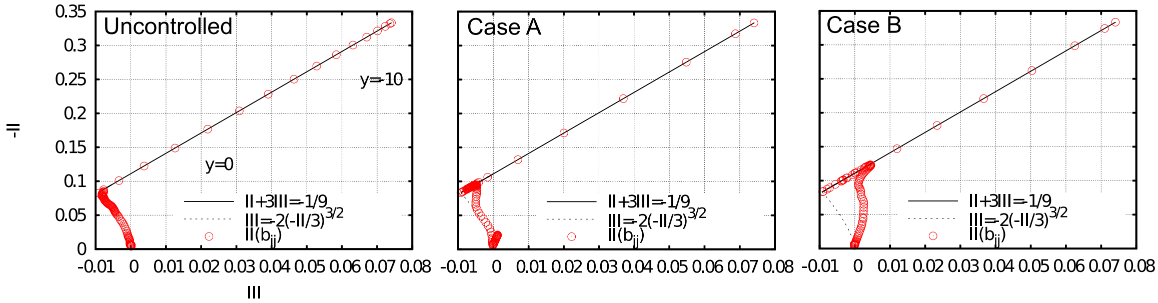

Figure 10. The second and third invariants of anisotropy tensor at $x = 6.9$: left, uncontrolled case; center, Case A; right, Case B.

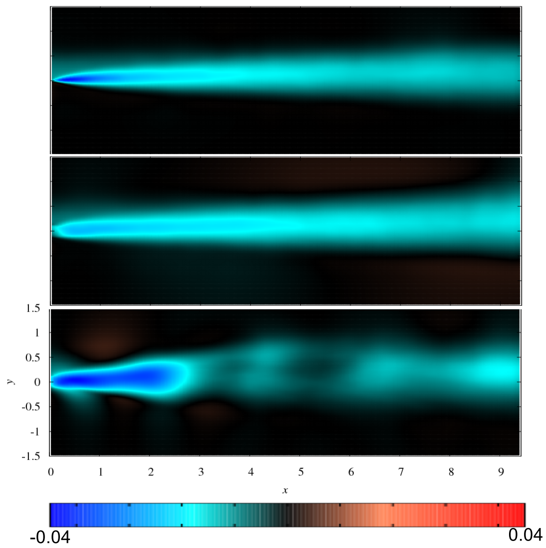

Figure 9. Reynolds shear stress, $\overline{u'v'}$: top, uncontrolled case; middle, Case A; bottom, Case B.

REFERENCES

Brown, G. L. & Roshko, A. 1974 On density effects and late structure in turbulent mixing layers. *J. Fluid Mech.* **64**, 775–816.

Brown, G. L. & Roshko, A. 2009 Turbulent shear layers and wakes. *J. Turbulence* **13**, N51.

Fukagata, K., Kasagi, N. & Koumoutsakos, P. 2006 A theoretical prediction of friction drag reduction in turbulent flow by superhydrophobic surfaces. *Phys. Fluids* **18**, 051703.

Ham, F. E., Lien, F. S. & B., Strong A. 2002 A fully conservative second-order finite difference scheme for incompressible flow on nonuniform grids. *J. Comput. Phys.* **177**, 117–133.

Ho, C. M. 1982 Subharmonics and vortex merging in mixing layers. *J. Fluid Mech.* **119**, 443–473.

Huang, L. S. & Ho, C. M. 1990 Small-scale transition in a plane mixing layer. *J. Fluid Mech.* **210**, 475–500.

Kametani, Y. & Fukagata, K. 2011 Direct numerical simulation of spatially developing turbulent boundary layers with uniform blowing or suction. *J. Fluid Mech.* **681**, 154–172.

Lund, T.S., Wu, X. & Squires, K. D. 1998 Generation of turbulent inflow data for spatially-developing boundary layer simulations. *J. Comput. Phys.* **140**, 233–258.

Miyauchi, T., Tanahashi, M. & Suzuki, M. 1996 Inflow and outflow boundary conditions for direct numerical simulations. *JSME Int. J. Ser. B* **39**, 305–314.

Naka, Y., Tsuboi, K., Kametani, Y., Fukagata, K. & Obi, S. 2010 Near-field development of turbulent mixing layer periodically forced by a bimorph pvdf film actuator. *J. Fluid Sci. Technol.* **5**, 156–168.

Spalart, P. R., Moser, R. D. & Rogers, M. M. 1991 A theoretical prediction of friction drag reduction in turbulent flow by superhydrophobic surfaces. *J. Comput. Phys.* **96**, 297–324.